Monopole antenna arrays for optical trapping, spectroscopy, and sensing

A. E. Çetin,[1] Ahmet Ali Yanik,[1] Cihan Yilmaz,[2] Sivasubramanian Somu,[2] Ahmed Busnaina,[2] and Hatice Altug[1,a)]
[1]*Department of Electrical and Computer Engineering, Boston University, Boston, Massachusetts 02215, USA and Photonics Center, Boston University, Boston, Massachusetts 02215, USA*
[2]*NSF Nanoscale Science and Engineering Center for High-rate Nanomanufacturing, Northeastern University, Boston, Massachusetts 02215, USA*

(Received 21 December 2010; accepted 3 February 2011; published online 17 March 2011)

We introduce a nanoplasmonic platform merging multiple modalities for optical trapping, nanospectroscopy, and biosensing applications. Our platform is based on surface plasmon polariton driven monopole antenna arrays combining complementary strengths of localized and extended surface plasmons. Tailoring of spectrally narrow resonances lead to large index sensitivities (S $\sim$675 nm/RIU) with record high figure of merits (FOM$\sim$112.5). These monopole antennas supporting strong light localization with easily accessible near-field enhanced hotspots are suitable for vibrational nanospectroscopy and optical trapping. Strong optical forces (350 pN/W/μm^2) are shown at these hotspots enabling directional control with incident light polarization. © *2011 American Institute of Physics*. [doi:10.1063/1.3559620]

Surface confinement of light through propagating and localized surface plasmons (SPs) holds great promise for applications in biosensing,[1,2] nanospectroscopy,[3–5] and optical trapping of bioparticles.[6,7] Within the past decade, many groundbreaking observations are demonstrated using metallic nanostructures. Plasmonic biosensors with high multiplexing characteristics are shown.[8] Ultrasensitive vibrational nanospectroscopy down to zepto-mole levels of proteins is demonstrated by using surface enhanced absorption signals amplified with collective plasmonic excitations.[9] Low-power plasmonic tweezers with minute trapping volumes well below the diffraction limited volume of light are realized with low power laser sources.[10] However, most of these plasmonic structures serve for a single operational purpose. For example, biosensing platforms based on effective refractive index modulation are not very suitable for spectroscopic applications since the near-field enhancements are relatively smaller than the nanoparticle based approaches with sharp structural features. On the other hand, plasmonic structures used for nanoparticle trapping are equipped with high gradient electromagnetic near-fields suitable for creating large transverse gradient forces, but lack spectrally sharp resonant behavior needed for sensing applications.

In this letter, we present a plasmonic platform merging multiple modalities by bringing complementary characteristics of localized and extended SPs together. The proposed platform, based on periodic arrays of nanopillars on a single metal sheet, allows enhanced device performances for biosensing, nanospectroscopy, and optical trapping applications at the same time. We achieve high refractive index sensitivities (S$\sim$675 nm/RIU) with large figure of merits (FOM $\sim$112.5) for detection limits. Such large figures are attributed to tight localization of plasmonic excitations in nanopillar structures leading to spectrally narrow resonances. Plasmonic hot spots created at the tips of the nanopillar structures are easily accessible by biochemical analytes, which is important for ultrasensitive spectroscopic measurements and optical trapping of nanoparticles with low power excitation sources. Polarization dependent optical force gradient enabled by the nanopillar arrays also provides the ability to control the direction of the trapping force. This platform, allowing optical trapping of bioparticles and simultaneous measurement of spectroscopic signatures and real time biodetection events, could find wide range of applications in sensing applications.

The monopole antenna array based nanopillar structures is illustrated in Fig. 1(a). The geometrical parameters of the system are the height (H) and radius (r) of the nanopillar and also the periodicity (P) of the array. The gold nanopillars stand on a gold plate with 150 nm thickness on top of a 500-nm-thick SiO_2 substrate. The illumination source perpendicular to the structure is polarized at x-direction. Numerical analysis is performed through finite-difference-time-domain (FDTD) simulations. In our simulations, Drude parameters are used for the gold nanostructures as reported in Ref. 11. To realize large scale fabrication of these nanostructures, a directed assembly process of nanoparticles as shown in Fig. 1(c) can be utilized. The assembly process is lift-off free, low cost, nonvacuum based, and simple compared to existing microfabrication techniques.[12] In this pro-

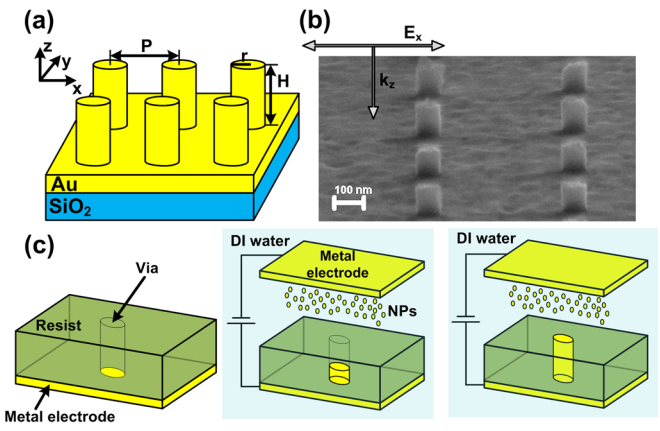

FIG. 1. (Color online) (a) Geometry of the nanopillar arrays. (b) SEM image of the nanopillar array with r=50 nm, H=100 nm, and P=500 nm. The direction of propagation and polarization of the illumination source is indicated in the figure. (c) Fabrication process of the nanopillar arrays.

a)Electronic mail: altug@bu.edu.

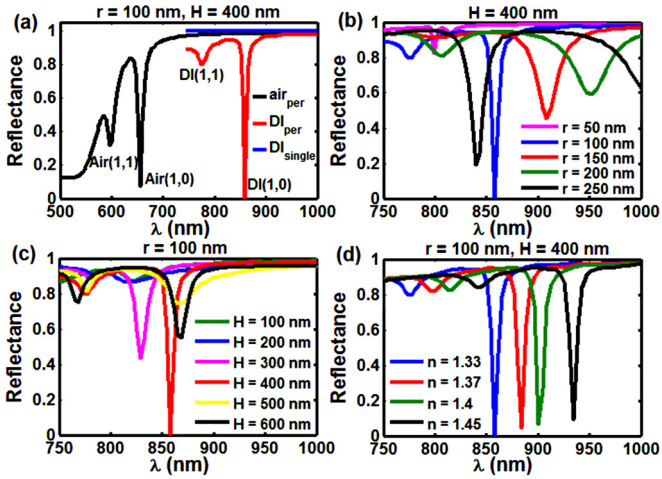

FIG. 2. (Color online) (a) The comparison of the free standing periodic system (r=100 nm, H=400 nm, and P=600 nm) with the single and periodic nanopillar systems in DI water. The SP modes for periodic structures are indicated in the figure. (b) Nanopillar arrays for different r values at fixed H (=400 nm) and P (=600 nm) at DI water. (c) Nanopillar arrays for different H values at fixed r (=100 nm) and P (=600 nm) at DI water. (d) Nanopillar arrays embedded in solutions with different n for corresponding parameters, r=100 nm, H=400 nm, and P=600 nm.

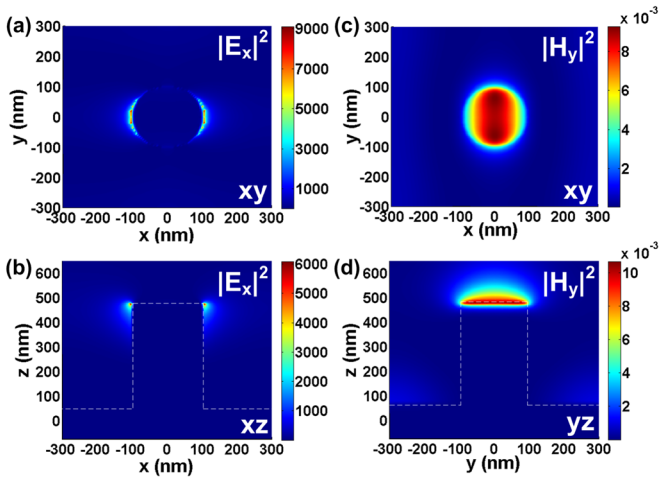

FIG. 3. (Color online) Intensity distributions of the system embedded in DI water for the x-component of E-field and the y-component of H-field with different cross-sections. The corresponding parameters are r=100 nm, H=400 nm, and P=600 nm. (xy)cross-section is determined at the top surface of the nanopillar. The position of the rod is indicated by white dashed line for xz and yz cross-sections.

cess, initially, gold layer is deposited on a glass substrate. Subsequently, nanoscale vias are fabricated with conventional electron-beam nanolithography using poly-methyl methacrylate (PMMA) resist. Then, metallic nanoparticles suspended in de-ionized (DI) water are precisely assembled into the vias by applying an electric field between the fixed bottom electrode and a top counter electrode placed far away from the resist. The dimension of fabricated nanopillars is controlled by the size of the vias. During the assembly process, nanoparticles are fused due to the current passing through them resulting in nanopillar formation in the vias. As a final step in the fabrication, the resist is dissolved using acetone. With this process, we can fabricate tall as well as high-aspect ratio nanopillars. Figure 1(b) shows scanning electron microscope (SEM) image of a preliminary result of a fabricated nanopillar array (r=50 nm, H=100 nm, and P=500 nm) employing the directed assembly process. The fabrication of a three-dimensional (3D) nanopillar array platform for optical measurements needs further developments to scale the nanopillar height to the optimized values.

Figure 2(a) shows the strong role of the localized and the extended SP couplings in periodic nanopillar array response. In periodic arrays, two resonance dips in the reflection spectra are observed corresponding to excitation of the SP polaritons (SPPs) by different grating orders. The relatively sharper and stronger resonance dip observed at longer wavelengths is due to the monopole antenna behavior of the nanopillar structure driven by the Au/DI(1,0) SPP excitation. The weaker resonance dip, on the other hand, is due to the excitation of the Au/DI(1,1) mode. It is also important to note that our nanopillar array is excited with perpendicularly illuminated light source. Unlike previous offerings based on prism coupling, this collinear arrangement enables massive multiplexing with minimal alignment requirements.[3] For the single nanopillar structure, resonances are not observable due to the weak coupling of the directly incident light. This observation proves the important role of SPPs in excitation of strong monopole antenna resonances in these structures. Figure 2(b) shows the radius dependence of resonance behavior of nanopillar arrays for a fixed height (H=400 nm) in DI water (n=1.33). Structures with small radiuses, i.e., r=50 nm, exhibit weak resonance behaviors, since the polarizability of the small nanopillars is relatively weaker. As the radius of the nanopillars increases, larger polarizability of the pillars enables stronger coupling of the SPPs to localized SPs (LSPs). An optimum resonance behavior with a spectrally sharp reflectance dip is observed when the radius of the structures is r=100 nm. Further increasing of nanopillar radius leads to redshifting in both Au/DI(1,0) and Au/DI(1,1) resonance modes as the LSPs shift to longer wavelengths. However, larger dimensions also lead to broader resonances due to increased losses.

As shown in Fig. 2(c), increasing height of the nanostructures (with a fixed radius of r=100 nm) results in redshifting in the plasmonic resonance dips. Optimum monopolar antenna behavior with nearly zero reflectance is observed when the height of the nanopillars is H=400 nm. As the length of the nanopillars further increases, the resonance gets broadened and reflectance dips become smaller. In the following analysis, nanopillar arrays with r=100 nm and H=400 nm are used since the best monopole antenna behavior with minimum reflectance and narrowest resonance line widths is observed for these structure parameters. The fabrication scheme described above is suitable for achieving the proposed structure. An optimized periodicity P=600 nm resulted with the sharpest resonance behavior. Figure 2(d) shows the resonance shifts for varying indexes of bulk solutions for the optimized arrays. As large as 675 nm/RIU ($S=\Delta\lambda/\Delta n$) refractive index sensitivity is achieved for these structures. For the optimized structure with spectrally narrow resonances (FWHM=6 nm), we showed that FOMs can be as large as 112.5. These values are more an order of magnitude larger than the previously recorded FOMs for nanoparticle and metamaterial sensors based on localized SPs.[13,14]

Figure 3 shows the near-field intensity distribution of the E_x and H_y field components for monopole antenna resonance of the optimized array excited through the Au/DI(1,0) SPP mode. Plasmonic excitations lead to dipolar E_x field distribution around the rims of the nanopillar structure at the top

surface with enhancement factors close to 9000 [Fig. 3(a)]. Monopolar antenna behavior is clearly observable in the xz-cross sectional field profile cutting through the center of this structure [Fig. 3(b)]. As shown in Figs. 3(c) and 3(d), near-field profile of H_y field component demonstrates strong near-field enhancements on the top surface of the pillar structure penetrating into the dielectric medium right above it. Strong near-field intensities extending into medium are ideal for enhanced vibrational spectroscopy applications as we can have maximum overlap between the analyte and the optical field. This characteristic is also highly suitable for optical trapping.

Optical forces can be obtained by integrating Maxwell stress tensor over an area surrounding a nanoparticle. In Figs. 4(a) and 4(b), 3D and two-dimensional (2D) illustrations are presented for three different locations of a dielectric spherical bead (radius 50 nm) where the optical forces are calculated within the near field of pillar structure. For all configurations, the center of the bead is positioned 200 nm above the top surface of the nanopillar structure (in z-direction). The x-y locations are chosen in a way that the bead is located always on an arc (radius 200 nm) centered at the nanopillar axis. Subsequently, the following three settings are chosen: (i) bead is located on the y-axis (blue colored). (ii) bead is located on the diagonal of the x-y axes (red colored). (iii) bead is located on the x-axis (black colored). In Fig. 4(c), different components of the optical forces acting on a bead are compared for different locations. Due to the dipolar mode character of the nanopillar LPs, the near-field gradients are symmetric in the x-direction when illuminated with an x-polarized light source. Hence, F_x component is zero for a bead located at (i). Similarly, F_y component is zero for a bead located at (iii). Both x- and y-direction force components exist for a bead located on the diagonal (ii). The stronger optical force in the y-direction ($F_x > F_y$) pulls the diagonally located bead (ii) toward the hotspot where the near-field gradients are expected to be largest. The strongest optical force is obtained once the bead is located at (iii) with $F_z = 350\ \mathrm{pN/W/\mu m^2}$, due to the direction of the propagation and the polarization of the illumination source. The ability to control the locations of the hotspots with the polarization of the incident light source also allows tunability of the optical gradient force. This strong and directional optical force can be utilized for optical trapping applications with polarization control.

In conclusion, we present a periodic gold nanopillar system merging multiple modalities by bringing complementary characteristics of localized and extended SPs together. The proposed platform which allows light coupling through the perpendicularly incident light could be advantageous for multiplexing applications. The platform enables high refractive index sensing measurements (675 nm/RIU) with very sharp resonance behavior (FWHM=6 nm). As a result, it offers large FOMs (FOM=112.5), which is an order of magnitude larger than the previously recorded FOMs for nanoparticle and metamaterial sensors based on localized SPs. Large near-field intensities (with enhancement factors close to 9000) that are easily accessible to biochemical analytes are shown for surface enhanced Raman spectroscopy measurements. Strong optical forces as high as $350\ \mathrm{pN/W/\mu m^2}$ are achieved around the hotspots. These strong and directional forces around the hotspots also allow directional control of the optical forces with the incident light polarization. Our platform, integrating multiple sensing modalities, including biosensing, spectroscopy and optical trapping in a compact form could find wide range of applications.

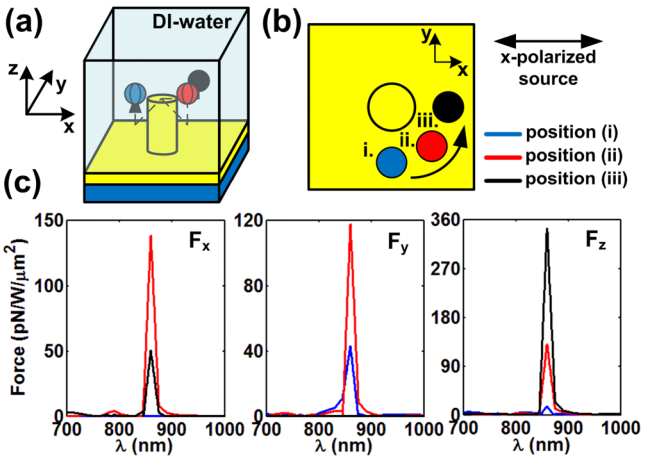

FIG. 4. (Color online) (a) 3D-schematic view of the structure with three beads with n=1.5 positioned differently inserted in DI-water. (b) 2D-view of the structure with the beads. (c) x-, y-, and z-component of the optical gradient force for three beads. The corresponding parameters are r =100 nm, H=400 nm, and P=600 nm.

This work is supported by National Science Foundation CAREER Award (ECCS-0954790) Engineering Research Center on Smart Lighting (EEC-0812056), NSF Grant No. 0832785, as well as by ONR Young Investigator Award, Massachusetts Life Science Center New Investigator Award. Authors acknowledge Kostas Research Center at Northeastern University and Boston University Photonics Center.

[1]A. V. Kabashin, Nature Mater. **8**, 867 (2009).
[2]A. A. Yanik, M. Huang, A. Artar, T.-Y. Chang, and H. Altug, Appl. Phys. Lett. **96**, 021101 (2010).
[3]V. Liberman, C. Yilmaz, T. M. Bloomstein, S. Somu, Y. Echegoyen, A. Busnaina, S. G. Cann, K. E. Krohn, M. F. Marchant, and M. Rothschild, Adv. Mater. (Weinheim, Ger.) **22**, 4298 (2010).
[4]Z. Huang, G. Meng, Q. Huang, Y. Yanh, and C. Zhu, Adv. Mater. (Weinheim, Ger.) **22**, 4136 (2010).
[5]S. Wang, D. F. P. Pile, C. Sun, and X. Zhang, Nano Lett. **7**, 1076 (2007).
[6]L. Huang, S. J. Maerkl, and O. J. F. Martin, Opt. Express **17**, 6018 (2009).
[7]V. D. Miljkovic, T. Pakizeh, B. Sepulveda, P. Johansson, and M. Kall, J. Phys. Chem. C **114**, 7472 (2010).
[8]J. N. Anker, W. P. Hall, O. Lyandres, N. C. Shah, J. Zhao, and R. P. V. Duyne, Nature Mater. **7**, 442 (2008).
[9]R. Adato, A. A. Yanik, J. J. Amsden, D. L. Kaplan, F. G. Omenetto, M. K. Hong, S. Erramilli, and H. Altug, Proc. Natl. Acad. Sci. U.S.A. **106**, 19227 (2009).
[10]A. N. Grigorenko, N. W. Roberts, M. R. Dickinson, and Y. Zhang, Nat. Photonics **2**, 365 (2008).
[11]E. D. Palik, *Handbook of Optical Constants of Solids* (Academic, Orlando, FL, 1985).
[12]C. Yilmaz, T.-H. Kim, S. Somu, and A. Busnaina, IEEE Trans. Nanotechnol. **9**, 653 (2010).
[13]N. A. Mirin, K. Bao, and P. Nordlander, J. Phys. Chem. A **113**, 4028 (2009).
[14]H. Liao, C. L. Nehl, and J. H. Hafner, Nanomedicine **1**, 201 (2006).